LANGMUIR Article
Cite This: Langmuir XXXX, XXX, XXX−XXX
pubs.acs.org/Langmuir

Impact of Electric Fields on the Nanoscale Behavior of Lipid Monolayers at the Surface of Graphite in Solution

Hongmei Bi,[†] Xuejing Wang,[‡] Xiaojun Han,*[,‡] and Kislon Voïtchovsky*[,§]

[†]College of Science, Heilongjiang Bayi Agricultural University, Daqing 163319, China
[‡]State Key Laboratory of Urban Water Resource and Environment, School of Chemistry and Chemical Engineering, Harbin Institute of Technology, Harbin 150001, China
[§]Department of Physics, Durham University, Durham DH1 3LE, U.K.

Supporting Information

ABSTRACT: The nanoscale organization and dynamics of lipid molecules in self-assembled membranes is central to the biological function of cells and in the technological development of synthetic lipid structures as well as in devices such as biosensors. Here, we explore the nanoscale molecular arrangement and dynamics of lipids assembled in monolayers at the surface of highly ordered pyrolytic graphite (HOPG), in different ionic solutions, and under electrical potentials. Using a combination of atomic force microscopy and fluorescence recovery after photobleaching, we show that HOPG is able to support fully formed and fluid lipid membranes, but mesoscale order and corrugations can be observed depending on the type of the lipid considered (1,2-dioleoyl-*sn*-glycero-3-phosphocholine, 1,2-dioleoyl-*sn*-glycero-3-phospho-L-serine (DOPS), and 1,2-dioleoyl-3-trimethylammoniumpropane) and the ion present (Na^+, Ca^{2+}, Cl^-). Interfacial solvation forces and ion-specific effects dominate over the electrostatic changes induced by moderate electric fields (±1.0 V vs Ag/AgCl reference electrode) with particularly marked effects in the presence of calcium, and for DOPS. Our results provide insights into the interplay between the molecular, ionic, and electrostatic interactions and the formation of dynamical ordered structures in fluid lipid membranes.

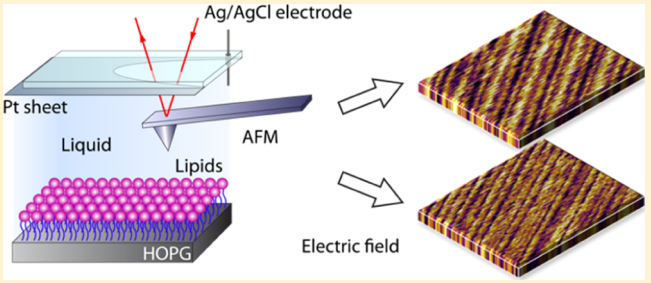

1. INTRODUCTION

Biological membranes (biomembranes) are primarily composed of lipids and membrane proteins self-assembled into a complex two-dimensional structure that can evolve in response to external stimuli and actively support the cell function.[1] By efficiently separating the inside of the cell from the surrounding environment, biomembranes are able to actively sustain a significant transmembrane electrical potential, the primary source of energy for the cell. This transmembrane potential also plays an important role in protein function[2,3] as well as the activation of many biological processes.[4] Additionally, as many membrane components are electrically charged, external electric fields can provide a driving force for the motion of components based on electrophoresis, electroosmosis, and hydrodynamic flow.[5−9] The central role of biological membranes in cell function is underlined by the fact that they constitute a primary drug target,[10] and countless studies have investigated the functional aspects of the nanoscale organization of different proteins and lipids.[11,12] However, the complexity and delicate nature of most native membranes render in situ nanoscale studies challenging, especially when considering the phenomena related to ionic effects[13−15] and to the transmembrane potential. To date, few studies have been able to explore the molecular-level details of membranes under an electrical potential, and investigations are typically conducted on membrane fragments or synthetic model membranes supported on a flat solid.[16,17] Changes in the membrane molecular assembly and the structure of its components in response to electric fields can provide important clues about how the transmembrane potentials impact the behavior and function of living cells. The use of supported membranes is particularly helpful for high-resolution studies because it limits the spatial fluctuations natural to cell membranes, and the support can be directly used as an electrode for imposing a controlled transmembrane potential.[18,19] Supported membranes are routinely used as model systems for nanoscale investigations with techniques such as fluorescence and super-resolution microscopies[20] and atomic force microscopy (AFM).[21,22] AFM can simultaneously offer molecular-level topographical and mechanical information about the membranes;[23−25] it can be combined with most optical microscopies and is fully compatible with the electrochemical measurements on membranes.[26−29]

The details of the electrochemical behavior of model membranes and lipid bilayers assembled on gold substrates have already been reported,[30−35] also using AFM.[14−16,33−38]

Received: May 16, 2018
Revised: June 29, 2018
Published: July 20, 2018

The results have shown a potential-induced slow structural transformation of the membrane until a characteristic corrugated phase appears.[36] The overall stability of the membrane depends on the magnitude of the applied electrical potential; studies with model 1,2-dimyristoyl-*sn*-glycero-3-phosphocholine−cholesterol bilayers[21] demonstrated a stability limit of −0.3 V, with membrane swelling observed beyond −1.0 V. The results are however dependent on the membrane composition, and AFM spectroscopy on lipid bilayers with increasing ganglioside content[37] showed a transition from a corrugated to a homogeneous phase, with an associated increase in the bilayer thickness (from ∼5.3 to 7.3 nm). The use of gold electrodes can be problematic in the context of biomembranes, first because biomolecules tend to adhere nonspecifically to gold, often resulting in the deformation or denaturation of the molecules.[38−40] Additionally, the fabrication of gold electrodes makes it often difficult to achieve a large area that is atomically flat. The surface of the electrode is typically composed of multiple small crystals exposing the Au(111) facet and able to reconstruct rapidly in ambient conditions.[21,33,37,41,42] There are examples of measurements with polycrystalline gold electrodes exhibiting large surfaces of Au(111) and good bilayer stability,[43] but these are not the norms. These issues can be overcome with liquid metal mercury electrodes. This strategy has been successfully used for developing fundamental theories about the phase behavior of lipids under electric fields[44−46] and investigating the channel transport of ions.[47−54] Various experimental strategies have been reported, such as the use of wafer-based mercury film electrodes,[55,56] the tracking of phase transition at different potentials using silver/silver chloride (Ag/AgCl),[57] or the recent direct measurement of the structural changes of lipid layers at electrified Hg surfaces using AFM spectroscopy.[58] Despite these successes, working with mercury electrodes remains highly challenging; the electrodes are inherently fragile, and their long-term stability is uncertain. This renders the characterization of the membranes' electrochemical behavior with microscopic techniques particularly difficult.[51,59] Graphite offers a practical and cost-effective alternative to noble metal electrodes. Highly oriented pyrolytic graphite (HOPG) can be easily cleaved immediately before an experiment, revealing an atomically flat, highly conducting, inert, and clean surface spanning hundreds of micrometers. This makes HOPG as an excellent substrate for electrochemical AFM measurements, with examples spanning from the self-assembly of peptides[60−62] to single atom or ion investigations.[63−67] Yet, to the best of our knowledge, HOPG has never been used for the AFM investigations of lipid membranes under electric potentials. This may be due to the fact that HOPG is hydrophobic, hence allowing only the formation of a single lipid monolayer on its surface. However, this can be seen as an advantage for the investigation of nanoscale interfacial effects between the surface of bilayers and the surrounding solution because it ensures optimal stability of the supported layer.

In this work, we characterize the nanoscale structural changes of model lipid membranes supported on the basal plane of HOPG under electrical potentials using AFM and explore the effect of the field in controlling the resulting lipid assembly. We conduct high-resolution imaging and force spectroscopy measurements on pure phospholipid monolayers with zwitterionic (phosphocholine), negatively charged (phosphoserine), and positively charged (trimethylammonium−propane) headgroups. The AFM results are complemented by fluorescence recovery after photobleaching (FRAP) measurements, quantifying the lipid mobility in the absence of an electric field to confirm that the HOPG support does not significantly affect the properties of the lipids at rest.

2. EXPERIMENTAL SECTION

2.1. Materials. Neutral lipids (1,2-dioleoyl-*sn*-glycero-3-phosphocholine, DOPC), negatively charged lipids (1,2-dioleoyl-*sn*-glycero-3-phospho-L-serine, DOPS), and positively charged lipids (1,2-dioleoyl-3-trimethylammoniumpropane, DOTAP) were purchased from Avanti Polar Lipids (Alabaster, USA) with purity >99%. All other reagents were of analytical grade and purchased from Sigma-Aldrich (Gillingham, UK). The imaging solutions (150 mM NaCl and 150 mM $CaCl_2$) were prepared with ultrapure water (Milli-Q, 18.2 OM, <5 ppm organics, Merck-Millipore, Billerica, MA, USA).

2.2. Electrochemical System Setup. A bespoke electrochemical setup comprising three electrodes was developed for the experiments (Figure 1). The working electrode is made of HOPG (SPI Supplies, West Chester, PA) and acts as a support for the lipid monolayer. HOPG was glued with epoxy resin (Araldite, RS Components, UK) onto a stainless steel disk (SPI Supplies) for magnetic fixation to the AFM scanner, and an electrical contact was made directly to HOPG with a copper wire. The counter electrode was made of a thin platinum sheet (<1 μm thick, Gold Leaf Supplies, Bridgend, UK) uniformly covering the back of the AFM cantilever holder except for a hole directly above the cantilever (Figure 1).

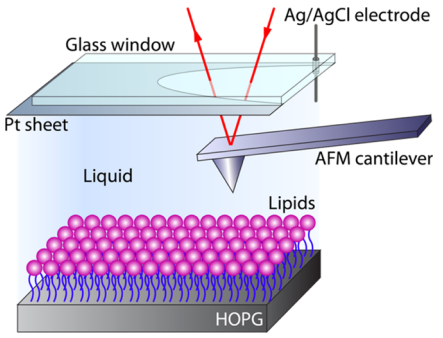

Figure 1. Schematic representation of the electrochemical AFM setup (not to scale). The HOPG substrate acts as the working electrode, the platinum sheet lining the glass window of the cantilever holder is the counter electrode, and the thin Ag/AgCl reference electrode is inserted through a hole located near the cantilever. The electric potential is applied by an Autolab electrochemical workstation.

This strategy ensured a uniform electric field while preventing any physical hindrance to the scanning tip and risk of short circuit. Additionally, the low cost of platinum sheets (typically <£0.1/cm^2 for high-purity Pt) allows for the routine replacement of the electrode if/when damaged. We used an Ag/AgCl reference electrode, prepared by electroplating a fresh Ag wire (75 μm diameter, Sigma-Aldrich, China) in 1.0 M KCl before every measurement. The current versus time curve of the Ag/AgCl reference electrode during this preparation (2 V applied potential) is shown in Figure S1. All potentials in this paper are quoted versus the potential of this reference electrode (0.235 V with respect to NHE) unless otherwise stated. The electrochemical measurements were conducted with an Autolab electrochemical workstation (PGSTAT204, Switzerland).

2.3. Sample Preparation. The supported lipid monolayers were formed via the vesicle fusion method.[67−70] In short, 2 mg of the desired lipids were dried overnight under vacuum in a glass vial and subsequently rehydrated in 1 mL of distilled water under ultrasound. Extrusion was conducted with a 100 nm filter (Whatman, GE Healthcare Life Sciences, Buckinghamshire, UK) using a mini-extruder kit (Avanti Polar Lipids). A mixture comprising 20 μL of

DOI: 10.1021/acs.langmuir.8b01631
Langmuir XXXX, XXX, XXX−XXX

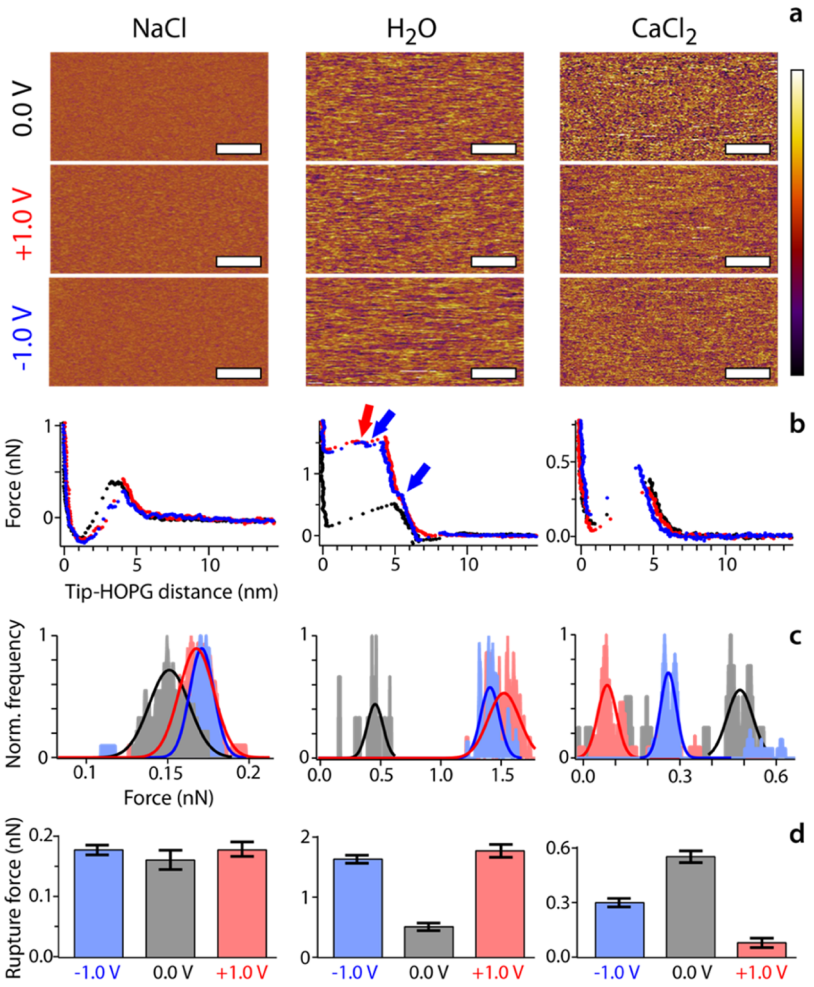

Figure 2. Impact of electric potentials on DOPC monolayers in different ionic solutions. In each solution, a representative topographic image is shown (a) and force−distance curve exhibiting membrane rupture (b) is shown for the applied potentials of 0 V (black), −1.0 V (blue), and +1.0 V (red). Arrows in (b) indicate the substeps in the monolayer rupture process. Statistical analysis of >10 force−distance curves (c) reveals the most probable rupture force and its variability in each case (see Supporting Information Figure S2 for a detailed description of the statistical analysis). A Gaussian fit of the main peak is also shown. The value of the average rupture force derived from the fit is shown in (d). The displayed error is the derived width of the Gaussian from the fit. The scale bar is 20 nm in (a) and the color bar represents a height variation of 1.8 nm.

the extruded solution and 100 μL of 150 mM NaCl solution was deposited onto a freshly cleaved HOPG and allowed to incubate at room temperature for 40 min. The exposed surface of HOPG is overwhelmingly composed of its basal plane apart from occasional step edges. The sample was then gently rinsed with 2 mL of the desired solution (ultrapure water, 150 mM NaCl, or 150 mM $CaCl_2$). If necessary, more imaging solution was added before the experiment. The sample was then placed into the AFM imaging cell for a 20 min thermal equilibration period at 25.0 ± 0.1 °C, immediately followed by the experiment. Given the temperature of the experiments, all lipid membranes are expected to be in fluid phase when at rest. Generally, the membranes appear fully stable on the HOPG substrate, with no noticeable changes over the duration of the experiments and after storage for up to 6 h.

2.4. AFM Experiments. All AFM data were acquired on a Cypher ES system (Asylum Research, Santa Barbara, CA, USA), with the sample and the cantilever/tip fully immersed in the imaging solution.[71,72] The cantilevers used for the experiments (RC800 PSA, Olympus, Tokyo, Japan) have a nominal spring constant of 0.1 N/m. They were further calibrated using their thermal spectrum to ensure comparability of the force measurements. During imaging, the cantilever was oscillated using photothermal excitation (blue drive) for more accuracy and stability. The relatively low resonance frequency of the first eigenmode in solution (~4 kHz) renders low noise imaging difficult. The cantilever was hence generally driven at its second vibration eigenmode (~35 kHz in solution). All images were taken at a constant scan rate (lines per second) of 2.44 Hz. Force spectroscopy measurements were conducted with a tip approach velocity of 200 nm/s, and the maximum applied force was controlled with a trigger. The samples were kept at 25.0 ± 0.1 °C using an in-built temperature control system. The analysis of the AFM results was conducted in IGOR Pro (WaveMetrics, Lake Oswego, USA) using home-programmed routines. The membrane rupture force, derived from the force−distance spectroscopy measurements, was directly calculated using a semiautomated procedure able to identify the steps and combine the results from multiple curves into suitable histograms (see Supporting Information Figure S2 for a detailed example).

2.5. FRAP experiments. The FRAP measurements were conducted on HOPG-supported lipid monolayers to quantify the lipid mobility in each experimental condition. The monolayers are expected to be in fluid state. A fluorescently labeled lipid (DPPE-Rhod, Avanti Lipids) was added to the lipid monolayer (0.04%, molar ratio) during the vesicle formation. Its low concentration does not affect the overall lipid fluidity, but the rhodamine tag provides the fluorescence needed[63] for the mobility measurement. A confocal fluorescence microscope (Nikon UK, Kingston, UK) was used to image the monolayer in reflection mode and carry out FRAP measurements, after rinsing with a different solution. The fluorescence recovery was analyzed over a 20 × 20 μm^2 bleaching spot. At least three separate measurements were carried out for each sample and

DOI: 10.1021/acs.langmuir.8b01631
Langmuir XXXX, XXX, XXX−XXX

subsequently averaged so as to derive reliable and statistically meaningful results. The data analysis was conducted in ImageJ (version 1.44p).[73] The lateral diffusion coefficient D was calculated using the following equation:[70,74,75]

$$D = 0.224R^2/t_{1/2} \quad (1)$$

where D is in $\mu m^2/s$, R is the radius of the bleached spot in μm, and $t_{1/2}$ (s) is the half-life of fluorescence recovery. This formula takes into account a correction and fitting because of the geometry of bleaching.[63,76,77]

3. RESULTS AND DISCUSSION

3.1. AFM Measurements. Hereafter, the three different lipids (DOPC, DOPS, DOTAP) are investigated sequentially, each in different solutions and for the potentials of 0 and ±1.0 V applied to the HOPG working electrode. The electrochemical stability of the HOPG surface itself was first tested over the same potentials in 150 mM NaCl (Figure S3), confirming no degradation or noticeable changes in its atomic features.

3.1.1. Electrically Neutral Monolayers. Electrically neutral monolayers were prepared with zwitterionic DOPC lipids (see Experimental Section). The representative AFM micrographs of the monolayers obtained with the applied potentials of 0, −1.0, and +1.0 V are shown in Figure 2. In all cases, a topographic image of the membrane is presented, together with a typical example of a force−distance curve, in which the AFM tip is able to rupture the monolayer by pressing perpendicularly to its surface. A statistical analysis of the rupture forces derived from >10 curves (typically 30) is also shown with the histogram of the resulting average value and its spread. No obvious features such as domain or corrugation are visible in the topography, except for the occasional horizontal scanning streak characteristic of AFM over the fluid membranes. No obvious structural transformation of the membrane could be observed under the electric fields, and the DOPC membrane remained fully fluid over all our experimental conditions (25 °C). This contrasts with the previous reports of significant structural transformations of the phosphocholine-based bilayers on electrified gold electrodes.[21,78] Although the lipids used in the present system are expected to be more fluid, some structural rearrangements in the membrane are still present. The zwitterionic nature of the phosphocholine headgroup makes it polar and its orientation is sensitive to the electrostatic environment. This results in the local electric field being able to shift the average molecular arrangement in the membrane and the transition temperature of the phosphocholine bilayers.[79] Here, this translates into significant differences in the observed rupture force, depending on both the ionic environment and the applied electric field.

In NaCl, the impact of the applied potential is minimal with a slight increase (∼15%) of the rupture force at ±1.0 V. This changes dramatically in pure water because of the lack of electrostatic screening. In the absence of an applied potential, the rupture force increases by a factor ∼2, presumably because of the surface potential of the immersed tip (typically −60 mV).[80−83] We note that given the different experimental conditions and tip compared to NaCl, an absolute comparison of the rupture force values should be done with caution. Nonetheless, the impact of the applied potential (directly comparable) is significant, inducing an increase >250% of the rupture force for both ±1.0 V. Additionally, the membrane rupture process exhibits some substeps less than a nanometer wide (blue and red arrows), suggesting some structural rearrangement of the phosphocholine headgroup under the tip pressure. These results are consistent with the idea of electrically induced rearrangement of the lipid packing.[79] The results of the measurements in $CaCl_2$ exhibit a behavior closer to that in NaCl, but with lower rupture forces under the applied electric fields and an asymmetrical behavior at positive and negative biases, presumably reflecting the difference in valency between the Ca^{2+} cation and the Cl^- anion. A high rupture force variability was observed in the absence of applied fields, with the most common value (histogram maximum) exhibiting a larger rupture force than at ±1.0 V. This high variability may be due to the localized ionic effects inducing mesoscale order in the membrane,[63] but the present results do not allow for a clear conclusion.

A quick look at Figure 2b provides an idea of the apparent thickness of the DOPC membrane in each condition, ranging from ∼3 nm at 0 V to 4−5 nm under a potential (from top to bottom of the step). This thickness is larger than expected for a DOPC monolayer, and a naive interpretation would rather suggest a bilayer. However, the presence of a bilayer on HOPG is highly unlikely in solution because the associated free energy would be considerably higher than that for the lipids exposing their hydrophobic tail to the HOPG surface. The phospholipid bilayers typically rearrange into monolayers when in contact with a hydrophobic surface.[84] Alternatively, our results could indicate a triple lipid layer, with a bilayer directly on top of a monolayer at the interface with HOPG, but the ∼3 nm thickness observed in NaCl does not support this interpretation. Additionally, the intermediate steps visible in pure water when under an electrical potential are significantly smaller than the thickness of a monolayer, supporting rather some structural rearrangement of the lipid headgroups and the associated hydration landscape probed by the tip. In light of these observations, we believe that our results are best explained by the presence of a lipid monolayer, potentially appearing larger because of its hydration layers, and ionic effects are at play, especially when under an electrical potential. The hydrated ions are likely to influence the apparent membrane thickness and affect its hydration landscape, as illustrated by the ∼2 nm change in apparent membrane thickness between the NaCl solution and pure water. Additionally, the fact that the substrate is hydrophobic makes the absolute thickness measurements difficult because the tip progressively loses its hydration shell while pressing against HOPG after having punctured the membrane. The results obtained at 0 V suggest a hydration thickness of ∼1 nm (distance between zero and step minimum). In principle, statistical analysis of the apparent thickness at the rupture point is possible, but an approach similar to that used for extracting the rupture forces (Figure 2c) provided unreasonable results for the reasons described above (not shown).

Generally, although our results are best interpreted by having a single DOPC monolayer on the HOPG surface together with significant hydration/ionic effects, we cannot exclude other interpretations, and AFM-independent control experiments are needed to reach a definitive conclusion. We therefore conducted time-dependent electrical measurements (electrochemical impedance spectroscopy) on the system to quantify its capacitance (see Supporting Information Figure S4 for details). We investigated each of the three types of lipid membranes as well as HOPG for reference, always in a 150 mM NaCl solution. The results indicate resistance values of

DOI: 10.1021/acs.langmuir.8b01631
Langmuir XXXX, XXX, XXX−XXX

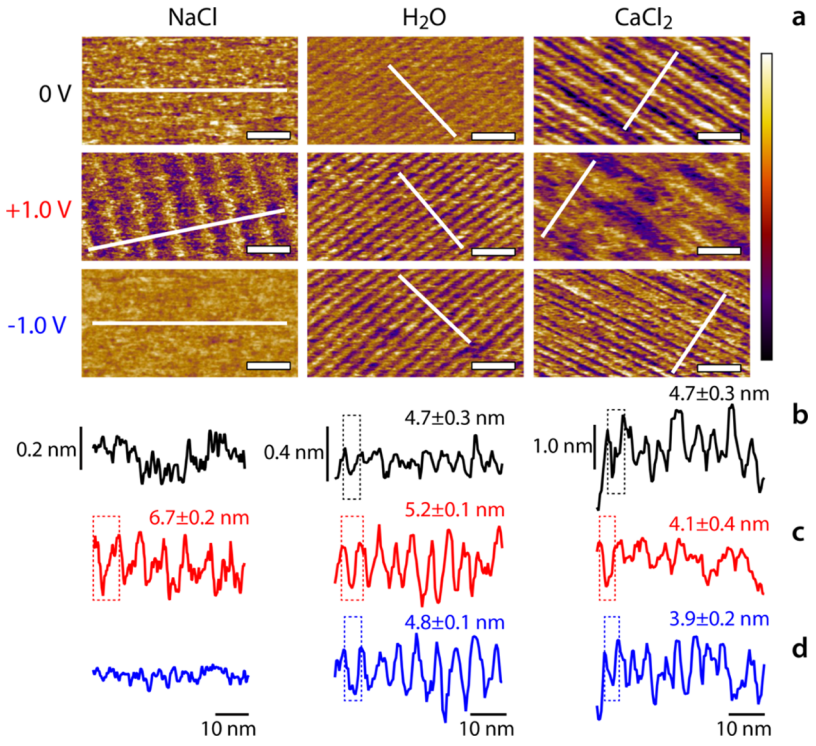

Figure 3. Impact of electric potentials on DOPS monolayers in different ionic solutions. In each solution, a representative topographic image is shown (a) together with a profile taken at 0 (b), +1.0 (c), and −1.0 V (d). For each profile exhibiting periodic corrugations, a single corrugation is highlighted (dashed box) and the average periodicity length is given in the inset. The scale bar is 20 nm in (a) and the color bar represents a height variation of 0.5 nm in NaCl, 1 nm in pure water, and 2.5 nm in $CaCl_2$.

172 kΩ for bare HOPG, 306 kΩ for DOPC, 316 kΩ for DOPS, and 477 kΩ for DOTAP, confirming the formation of lipid membranes on the HOPG substrate. However, the corresponding membrane capacitances were found to be 8.15 $\mu F/cm^2$ (DOPC), 8.46 $\mu F/cm^2$ (DOPS), and 9.48 $\mu F/cm^2$ (DOTAP), more than 4 times larger than that expected for a perfect monolayer. Indeed, the characteristic capacitance of lipid bilayers ranges from 0.4 to 1 $\mu F/cm^2$,[85,86] indicating that a monolayer capacitance should hence be typically ranging between 0.8 and 2 $\mu F/cm^2$. This high apparent capacitance can be explained by the defects in the monolayers, for example, at the step edges of HOPG because of its large surface area. The current leakage at these defects would artificially raise the observed capacitance values during the electrochemical impedance spectroscopy measurements, as observed here. In summary, although the impedance data tend to support the presence of a monolayer, it is also not fully conclusive.

3.1.2. Negatively Charged Lipid Monolayers. Negatively charged lipid monolayers were created from DOPS using the same protocol as for DOPC. Figure 3 shows the effect of the different saline solutions and electric fields on the membrane topography. Unlike DOPC, the phosphoserine headgroups of DOPS appear to influence dramatically the molecular organization of the lipids in the membrane, depending on the local electrostatic environment. The AFM micrographs reveal clear structural changes such as periodic corrugations in the form of parallel row-like features that could be observed in different experimental conditions (Figure 3a). These features are reminiscent of the hemimicellar lipid structures reported in previous reports.[87−90]

In NaCl, the membrane appears completely homogeneous at 0 and −1.0 V. When +1.0 V is applied to the HOPG electrode for about 15 min, faint corrugations with a periodicity of 6.7 ± 0.2 nm and a depth of ∼200 pm are occasionally visible, but they exhibit an unusual shape in sawtooth pattern, the symmetry of which depends on the scanning direction (trace or retrace, not shown). This indicates a tip-induced structuring of the membrane. A similar effect has previously been reported on DOPC membrane in specific ionic solutions able to reduce the lipid mobilities.[63] Here, these results suggest that positive potentials help structure the lipid molecules by attracting their headgroups to the membrane, hence limiting their mobility.[63] The dissolved ions do not appear to play a major role beyond the immediate screening of the charged phosphoserine group. The force−distance measurements did not show any sizeable rupture force (Supporting Information Figure S5), confirming a highly fluid membrane. An extensive rinsing of the membrane with ultrapure water revealed significant structural changes after ∼15 min equilibration. At 0 V, some corrugations ∼150 pm deep are already visible and do not depend on the tip scanning direction, suggesting that they represent intrinsic properties of the membrane in these conditions. Applying an electric potential of ±1.0 V results in corrugations similar in shape and periodicity, but significantly more marked with a depth often larger than 0.5 nm.

The most unusual features are seen in the $CaCl_2$ solution, in which some deep (∼2 nm) periodic corrugations are already apparent at 0 V. Interestingly, although the average periodicity between the usual row-like features is comparable to that observed in other solutions and conditions, the rows appear grouped three by three, creating higher-order corrugations with a periodicity of almost 20 nm. These superstructures appear completely novel and do not match the previous reports of hemimicellar lipid structures on Au(111).[87−90] The

DOI: 10.1021/acs.langmuir.8b01631
Langmuir XXXX, XXX, XXX−XXX

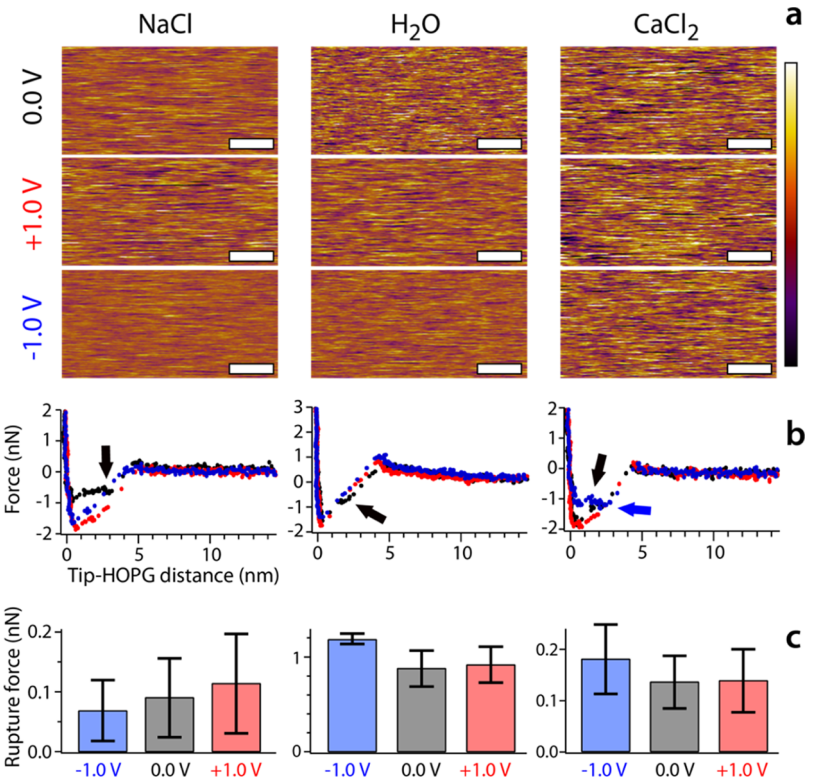

Figure 4. Impact of electric potentials on DOTAP monolayers in different ionic solutions. In each solution, a representative topographic image is shown (a) and force−distance curve exhibiting membrane rupture (b) is shown for the applied potentials of 0 V (black), −1.0 V, (blue) and +1.0 V (red). Arrows in (b) indicate the substeps in the monolayer rupture process. Statistical analysis of >10 force−distance curves reveals the most probable rupture force and its variability in each case (c). The displayed error is twice the width of the Gaussian fit (see Supporting Information Figure S2 for a detailed description of the statistical analysis). Scale bars are 20 nm. The color bar represents 1.8 nm height variation.

fact that these complex structures develop in $CaCl_2$ even in the absence of any applied potential indicate a direct effect of the divalent Ca^{2+} ions on the monolayer structure, presumably through the bridging of multiple lipid headgroups by a single cation. Ca^{2+} ions are indeed well-known to strongly bind phosphoserine lipids.[91] When a potential of +1.0 V is applied to the HOPG substrate for 15 min, the larger "super-corrugations" remain visible, but the smaller periodicity almost completely vanishes in places. Overall, the membrane appears more regular than under an open-circuit potential. In contrast, applying −1.0 V tends to partially remove the high-order supercorrugations, but the smaller row-like features appear more clearly with a depth comparable to that visible at 0 V. Altogether, the results with DOPS membranes show that both the ionic solution and the transmembrane electric potential can affect the lipid molecular assembly, creating some distinctive structural changes. The plausible molecular mechanisms underlying these changes will be detailed in the Results and Discussion section.

3.1.3. Positively Charged Lipid Membranes. Positively charged lipid membranes were formed from the DOTAP lipid that exhibits cationic trimethylammonium−propane headgroups. As for previous lipids, the membranes were examined in the three different ionic solutions and under electrical potentials, with the representative results shown comparatively in Figure 4. Unlike DOPS membranes, DOTAP membranes exhibit now distinctive features regardless of the imaging conditions, with the results reminiscent of images acquired in DOPC (Figure 2). This is not surprising given the fact that, except for the potential hydration effects related to each saline solution, Na^+ or Ca^{2+} cannot adsorb to the TAP headgroup and hence affect the DOTAP assembly. When comparing the solutions, the only difference with the direct consequences on the system's electrostatics is the removal of Cl^- ions in ultrapure water, in which OH^- ions are left to ensure electroneutrality. The only voltage-dependent effect visible in the images is a slight increase in the apparent membrane roughness in NaCl and water when a positive electric potential is applied, possibly because of a partial repulsion of DOTAP from HOPG. The effect is however subtle and the explanation is speculative.

More useful information can be derived from a statistical analysis of the membrane rupture force in each condition. In NaCl, the average rupture force is about an order of magnitude lower than in DOPC at all potentials. All the rupture forces are equal within error. The rupture substeps are occasionally visible (Figure 4), suggesting some specific ionic interactions or hydration effects between the dissolved ions and the TAP headgroups. In contrast, most substeps are gone in ultrapure water, except at 0 V. The average rupture force also increases significantly, suggesting that the lack of metal ions rigidifies the membrane. This could be due to direct electrostatic effects: diminished electrostatic screening between headgroups leading to an increased lateral tension within the two-dimensional confined membrane. However, the fact that the increase in rupture force occurs independently of the applied voltage suggests that the direct electrostatic interactions between lipid headgroups do not dominate the membrane cohesion; hydration effects may rather be at play. Consistently, the better electrostatic screening of the lipid headgroups at −1.0 V

DOI: 10.1021/acs.langmuir.8b01631
Langmuir XXXX, XXX, XXX−XXX

only marginally increases the observed rupture force, with no clear effect within error. In $CaCl_2$, the rupture force decreases again to values about double of those observed in NaCl. Again, the change occurs evenly at all potentials, and the rupture substeps reappear, consistent with the observations made in NaCl.

3.2. FRAP Measurements. FRAP measurements were conducted for all lipids in pure water and in all ionic solutions at different electrical potentials in DOPS. The aim is to complement the AFM measurements and help with the interpretation of AFM results, especially where the structural organization of lipids appears to have a significant impact. Reference FRAP measurements were conducted on DOPC, DOPS, and DOTAP membranes in ultrapure water. The derived lipid mobilities are summarized in Table 1. In each case, the estimated mobile fraction of the lipids is also given (see Materials and Supporting Information Figure S6 for more details).

Table 1. Lipid Mobilities in Ultrapure Water Calculated from FRAP Measurements

lipid	potential	mobility ($\mu m^2/s$)	mobile fraction (%)
DOPC	−1.0	0.86 ± 0.24	0.75
	0.0	0.89 ± 0.15	0.71
	+1.0	0.67 ± 0.24	0.63
DOPS	−1.0	1.86 ± 0.12	0.90
	0.0	1.11 ± 0.21	0.89
	+1.0	0.92 ± 0.25	0.87
DOTAP	−1.0	1.06 ± 0.28	0.81
	0.0	1.11 ± 0.13	0.88
	+1.0	1.35 ± 0.23	0.86

Both the fluidity and mobile fraction (recovery level) of DOPC are lower than that for charged lipids. Interestingly, although AFM experiments show significant corrugations and molecular ordering in DOPS membrane even in pure water, the DOPS mobility is still comparable to that of unstructured DOTAP membranes and higher than that for DOPC. This indicates that the corrugation structure observed in DOPS represents a dynamical equilibrium with the AFM picking up a time-average structure that still allows for excellent mobility, presumably because of the repulsion between DOPS and the slightly negatively charged HOPG at the open potential. This is also consistent with the low rupture forces measured in DOPS (Figure S5). The apparent difficulty for the DOPC molecules to diffuse freely on HOPG is also consistent with the remarkably large rupture forces observed (Figure 2), but slightly lower than the typical DOPC mobilities reported for bilayers.[92] It is well-known that the interactions with the supporting solid can locally order the contacting molecules and reduce their diffusion properties,[64,93−95] including for lipid membranes.[96,97] Here, the lack of lubrication water between a proximal leaflet and the solid support may be responsible for the lower lipid mobilities. Notwithstanding these details, we note that the lipid mobilities observed on HOPG confirm that all the lipid membranes remain fluid, with the lipid mobilities comparable to those reported for traditional supported bilayers. This is in itself a success of the approach used here. The FRAP measurements in DOPS were conducted in ionic solutions and under applied electrical potentials. The results are summarized in Table 2.

Table 2. DOPS Mobility in the Different Ionic Solutions Calculated from FRAP Measurements

solution	potential (V)	mobility ($\mu m^2/s$)	mobile fraction (%)
NaCl	−1.0	1.88 ± 0.12	0.89
	0.0	1.82 ± 0.17	0.87
	+1.0	1.03 ± 0.18	0.85
$CaCl_2$	−1.0	1.29 ± 0.26	0.87
	0.0	0.96 ± 0.24	0.85
	+1.0	0.87 ± 0.14	0.84

From Table 2, it is clear that the mobility of DOPS is the highest in the NaCl solution, followed by ultrapure water, and the lowest in $CaCl_2$. Electrical potentials appear to have a limited impact on the lipid mobility. This result is fully consistent with the AFM observations (Figure 3), whereby the more marked the membrane corrugations, the lowest is the lipid mobility. The fact that the membrane remains fluid in all conditions further supports the hypothesis that the AFM captures the time average of a dynamical molecular arrangement, in which the lipid molecules remain mobile. The mobilities are, however, affected by the ionic environment, suggesting that while the membranes remain fluid, environments inducing significant structural organization of the membrane will also reduce the lipid mobility. This result is similar to that reported recently by Piantanida et al. for DOPC bilayers on a hydrophilic substrate,[63] demonstrating the generality of ionic effects in modulating lipid membranes' mesoscale organization and mobility. The supporting solid has an influence on the equilibrium structures formed, with the longitudinal row consistent with the crystalline lattice of HOPG. However, it is the ions that primarily drive the clustering on lipid molecules, rendering the formation of structures possible in the first place.

4. GENERAL DISCUSSION

The AFM results and the FRAP measurements both show that HOPG is able to support the fluid lipid monolayers, with the properties and mobilities close to those of the standard supported lipid bilayers at rest (no potential).[92] When an electrical potential is applied, the monolayers can form some mesoscale molecular arrangements (corrugations) depending on the nature of the lipids, the ionic environment, and the applied transmembrane electric fields. Similar results have previously been reported for bilayers on metal electrodes,[18] again supporting HOPG as a suitable substrate for studying the electrochemical effects occurring at the interface between the lipid membranes and aqueous solutions.

Significantly, the results demonstrate that ionic effects dominate over electrical fields within the range of potentials investigated here, with the membrane rupture forces and patterns suggesting that field to fine-tuning the lipid's molecular arrangement. The electrical potential is also able to modulate the concentration of dissolved ions at the membrane−solution interface and hence indirectly influence the ionic effects.

DOPC and DOTAP membranes remain globally unstructured in most solutions and under potentials, whereas DOPS membranes exhibit striking features that indicate a significant degree of mesoscale lipid ordering. Figure 5 proposes a model of the molecular mechanisms responsible for the features reported in Figure 3. In NaCl (membrane deposition solution), the Na^+ ions ensure electroneutrality of the

DOI: 10.1021/acs.langmuir.8b01631
Langmuir XXXX, XXX, XXX−XXX

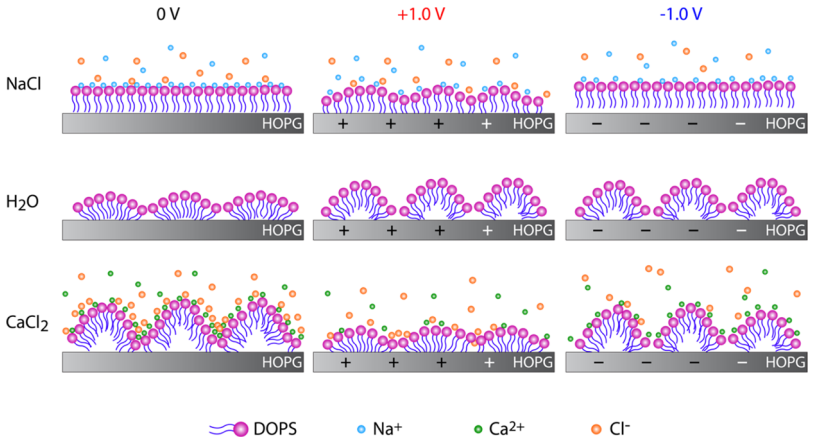

Figure 5. Schematic representation of the molecular organization of a DOPS monolayer on HOPG in different ionic environments and under electrical potentials. Not to scale.

headgroup (Figure 5, NaCl). Shallow corrugations are visible when +1.0 V is applied, presumably because of the attraction of Cl^- anions at the membrane−solution interface, thereby disrupting the existing hydration structure. The direct electrostatic attraction between the phosphoserine headgroups and HOPG may also play a role. Consistently, no corrugations are seen at −1.0 V. Subsequent rinsing with ultrapure water upsets the hydration structure of the membrane and its electrostatic balance, changing the lipid arrangement in the membrane. In the absence of potential, DOPS forms a hemimicelle-like arrangement reminiscent of detergents on HOPG.[98−100] Applying an electrical potential exacerbates the apparent amplitude of the corrugations but not their overall shape, suggesting a subtle effect involving water molecules and the lipid headgroups, as electrostatics alone cannot explain the symmetry between ±1.0 V (Figure 5, H_2O).

However, the increased lipid mobility at −1.0 V still suggests a global repulsion between the headgroups and the HOPG surface. Rinsing of the membrane with $CaCl_2$ solution led to larger corrugations (Figure 5, $CaCl_2$) with a clear and distinct impact of applied potentials. The spontaneous curvature at 0 V and the different responses to positive and negative potentials all point to Ca^{2+} ions dominating the system through specific interactions with the lipid headgroups. When +1.0 V is applied, partial desorption of Ca^{2+} cations blurs out the corrugations, whereas at −1.0 V the structures are reinforced, presumably because of a locally increased Ca^{2+} concentration. It is well-known that the electrically induced adsorption of ions in monolayers can influence the membrane phase transition[58] depending on the magnitude and sign of the potential.[57]

We note that the silicon oxide AFM tip is negatively charged in all the experimental conditions examined in this study. This negative surface potential can in principle impact the AFM measurements, in particular those of the rupture forces. This effect is unlikely to appreciably affect the measurements in ionic solutions because of the electrostatic screening of the tip by the dissolved ions. In ultrapure water, the electrostatic tip effects on the measured rupture forces can a priori not be excluded, for example, with the DOPC and DOTAP membranes. Direct electrostatic interactions between the tip and HOPG may also be at play. However, the hydration effects appear to dominate the direct electrostatics, and the applied potentials tend not to provide consistent differences with the open-circuit rupture forces. Additionally, the voltages imposed here are more than an order of magnitude larger than the surface potential of the tip, suggesting that the tip effects can be seen as a small perturbation of the system. We also note the consistency of the FRAP measurements with the AFM results, suggesting the latter to be reliable, at least with respect to the reported trends.

5. CONCLUSIONS

In this work, we investigate the nanoscale structure and dynamics of HOPG-supported phospholipid monolayers in different ionic solutions and under electrical potential. Combining AFM in liquid with FRAP measurements, we show that ions can induce mesoscale-ordered molecular structures within the lipid membrane, while retaining its fluidity. The experiments in NaCl, $CaCl_2$, and ultrapure water suggest that these effects are dominated by ion-mediated hydration forces, with the direct electrostatic interactions playing a secondary role while still present. Electric fields can influence the molecular organization, cohesion, and dynamics of the lipids in the membrane, but not as dramatically as ions, and in particular calcium, at least for the voltages explored here (±1.0 V). The results strongly depend on the type of lipid considered, with particularly marked effects in DOPS. In comparison, zwitterionic and cationic lipids showed little or no ordering effect aside from the changes in the membrane rupture force. Although the present study does not control the actual transmembrane potential, experiments imposing smaller voltages (400 mV) induced very similar membrane changes and molecular rearrangements, but requiring a longer equilibration time, consistently with previous studies.[90,101] Natural transmembrane potentials in biology typically have a comparable magnitude, ranging over few hundreds of millivolts. This suggests our results to be of relevance for natural biological systems, where transmembrane potentials may help control the lipid molecular arrangement and the membrane permeability. We believe our findings could have significant implications in the development of lab-on-a-chip lipid-based devices and for understanding the effect transmembrane potentials have on the molecular ordering of lipids in biological membranes, in particular with a view of mimicking biological electrochemical functions.

DOI: 10.1021/acs.langmuir.8b01631
Langmuir XXXX, XXX, XXX−XXX

■ ASSOCIATED CONTENT

Supporting Information

The Supporting Information is available free of charge on the ACS Publications website at DOI: 10.1021/acs.langmuir.8b01631.

Preparation procedures for the Ag/AgCl electrode, electrochemical impedance spectroscopy results, description of the procedure used to analyze AFM spectroscopy, example of rupture forces recorded for DOPS in NaCl solution, and representative FRAP experiments of lipids (PDF)

■ AUTHOR INFORMATION

Corresponding Authors

*E-mail: hanxiaojun@hit.edu.cn (X.H.).
*E-mail: kislon.voitchovsky@durham.ac.uk (K.V.).

ORCID

Xiaojun Han: 0000-0001-8571-6187
Kislon Voïtchovsky: 0000-0001-7760-4732

Author Contributions

H.B., X.H., and K.V. conceived the study and designed the experiments. H.B. conducted the measurements. X.W. supplemented some FRAP experiments. K.V. analyzed the AFM data. H.B. wrote the manuscript. X.H. and K.V. revised the manuscript.

Notes

The authors declare no competing financial interest.

■ ACKNOWLEDGMENTS

The authors thank William Trewby (Durham) for help with AFM measurements and Ethan J. Miller (Durham) for his assistance in the FRAP experiments. This research was supported by the National Natural Science Foundation of China (grant nos. 21503072, 21773050), Program of Introduction Talents in University (grant no. XDB-2017-19), and sponsored by China Scholarship Council (grant no. 20163035). K.V. acknowledges financial support from the Royal Society International Exchange program (IE140921), the Engineering and Physical Sciences Research Council (EP/M023915/1), and the European Council (MC CIG 631186).

■ REFERENCES

(1) Pignatello, R. Biological Membranes and Their Role in Physio-Pathological Conditions. In *Drug−Biomembrane Interaction Studies: The Application of Calorimetric Techniques*; Pignatello, R., Ed.; Woodhead Publ Ltd: Cambridge, 2013; pp 1−46.

(2) Orsini, F.; Migliaccio, E.; Moroni, M.; Contursi, C.; Raker, V. A.; Piccini, D.; Martin-Padura, I.; Pelliccia, G.; Trinei, M.; Bono, M.; Puri, C.; Tacchetti, C.; Ferrini, M.; Mannucci, R.; Nicoletti, I.; Lanfrancone, L.; Giorgio, M.; Pelicci, P. G. The Life Span Determinant P66Shc Localizes to Mitochondria Where it Associates with Mitochondrial Heat Shock Protein 70 and Regulates Transmembrane Potential. *J. Biol. Chem.* **2004**, *279*, 25689−25695.

(3) Strahl, H.; Hamoen, L. W. Membrane Potential is Important for Bacterial Cell Division. *Proc. Natl. Acad. Sci. U.S.A.* **2010**, *107*, 12281−12286.

(4) Yu, H.; Yzeiri, I.; Hou, B.; Chen, C.-H.; Bu, W.; Vanysek, P.; Chen, Y.-S.; Lin, B.; Král, P.; Schlossman, M. L. Electric Field Effect on Phospholipid Monolayers at an Aqueous-Organic Liquid-Liquid Interface. *J. Phys. Chem. B* **2015**, *119*, 9319−9334.

(5) Cheetham, M. R.; Bramble, J. P.; McMillan, D. G. G.; Krzeminski, L.; Han, X.; Johnson, B. R. G.; Bushby, R. J.; Olmsted, P. D.; Jeuken, L. J. C.; Marritt, S. J.; Butt, J. N.; Evans, S. D. Concentrating Membrane Proteins using Asymmetric Traps and AC Electric Fields. *J. Am. Chem. Soc.* **2011**, *133*, 6521−6524.

(6) Jönsson, P.; Beech, J. P.; Tegenfeldt, J. O.; Höök, F. Mechanical Behavior of a Supported Lipid Bilayer under External Shear Forces. *Langmuir* **2009**, *25*, 6279−6286.

(7) Jönsson, P.; Gunnarsson, A.; Höök, F. Accumulation and Separation of Membrane-Bound Proteins using Hydrodynamic Forces. *J. Am. Chem. Soc.* **2011**, *83*, 604−611.

(8) Han, X.; Cheetham, M. R.; Sheikh, K.; Olmsted, P. D.; Bushby, R. J.; Evans, S. D. Manipulation and Charge Determination of Proteins in Photopatterned Solid Supported Bilayers. *Integr. Biol.* **2009**, *1*, 205−211.

(9) Groves, J. T.; Boxer, S. G. Micropattern Formation in Supported Lipid Membranes. *Acc. Chem. Res.* **2002**, *35*, 149−157.

(10) Roth, J. S.; Zhang, Y.; Bao, P.; Cheetham, M. R.; Han, X.; Evans, S. D. Optimization of Brownian Ratchets for the Manipulation of Charged Components within Supported Lipid Bilayers. *Appl. Phys. Lett* **2015**, *106*, 183703.

(11) Pluhackova, K.; Böckmann, R. A. Biomembranes in Atomistic and Coarse-grained Simulations. *J. Phys.: Condens. Matter* **2015**, *27*, 323103.

(12) Fuentes, N. R.; Salinas, M. L.; Kim, E.; Chapkin, R. S. Emerging role of chemoprotective agents in the dynamic shaping of plasma membrane organization. *Biochim. Biophys. Acta, Biomembr.* **2017**, *1859*, 1668−1678.

(13) Voïtchovsky, K.; Antoranz Contera, S.; Kamihira, M.; Watts, A.; Ryan, J. F. Differential stiffness and lipid mobility in the leaflets of purple membranes. *Biophys. J.* **2006**, *90*, 2075−2085.

(14) Contera, S. A.; Voïtchovsky, K.; Ryan, J. F. Controlled ionic condensation at the surface of a native extremophilemembrane. *Nanoscale* **2010**, *2*, 222−229.

(15) Voïtchovsky, K.; Contera, S. A.; Ryan, J. F. Electrostatic and steric interactions determine bacteriorhodopsin single-molecule biomechanics. *Biophys. J.* **2007**, *93*, 2024−2037.

(16) Bao, P.; Cartron, M. L.; Sheikh, K. H.; Johnson, B. R. G.; Hunter, C. N.; Evans, S. D. Controlling Transmembrane Protein Concentration and Orientation in Supported Lipid Bilayers. *Chem. Commun.* **2017**, *53*, 4250−4253.

(17) Akbari, E.; Buntat, Z.; Shahraki, E.; Parvaz, R.; Kiani, M. J. Analytical Investigation of Bilayer Lipid Biosensor Based on Graphene. *J. Biomater. Appl.* **2016**, *30*, 677−685.

(18) Staffa, J. K.; Lorenz, L.; Stolarski, M.; Murgida, D. H.; Zebger, I.; Utesch, T.; Kozuch, J.; Hildebrandt, P. Determination of the Local Electric Field at Au/SAM Interfaces Using the Vibrational Stark Effect. *J. Phys. Chem. C* **2017**, *121*, 22274−22285.

(19) Madrid, E.; Horswell, S. L. Effect of Electric Field on Structure and Dynamics of Bilayers Formed From Anionic Phospholipids. *Electrochim. Acta* **2014**, *146*, 850−860.

(20) Kuo, C.; Hochstrasser, R. M. Super-resolution Microscopy of Lipid Bilayer Phases. *J. Am. Chem. Soc.* **2011**, *133*, 4664−4667.

(21) Chen, M.; Li, M.; Brosseau, C. L.; Lipkowski, J. AFM Studies of the Effect of Temperature and Electric Field on the Structure of a DMPC−Cholesterol Bilayer Supported on a Au(111) Electrode Surface. *Langmuir* **2009**, *25*, 1028−1037.

(22) Jeuken, L. J. C. AFM Study on the Electric-field Effects on Supported Bilayer Lipid Membranes. *Biophys. J.* **2008**, *94*, 4711−4717.

(23) Li, J. K.; Sullan, R. M. A.; Zou, S. Atomic Force Microscopy Force Mapping in the Study of Supported Lipid Bilayers†. *Langmuir* **2011**, *27*, 1308−1313.

(24) Yuan, J.; Hao, C.; Chen, M.; Berini, P.; Zou, S. Lipid Reassembly in Asymmetric Langmuir-Blodgett/Langmuir-Schaeffer Bilayers. *Langmuir* **2013**, *29*, 221−227.

(25) Bhojoo, U.; Chen, M.; Zou, S. Temperature induced lipid membrane restructuring and changes in nanomechanics. *Biochim. Biophys. Acta, Biomembr.* **2018**, *1860*, 700−709.

(26) Goksu, E. I.; Vanegas, J. M.; Blanchette, C. D.; Lin, W.-C.; Longo, M. L. AFM for Structure and Dynamics of Biomembranes. *Biochim. Biophys. Acta, Biomembr.* **2009**, *1788*, 254−266.

DOI: 10.1021/acs.langmuir.8b01631
Langmuir XXXX, XXX, XXX−XXX

(27) Lebègue, E.; Smida, H.; Flinois, T.; Vié, V.; Lagrost, C.; Barrière, F. An optimal surface concentration of pure cardiolipin deposited onto glassy carbon electrode promoting the direct electron transfer of cytochrome- c. *J. Electroanal. Chem.* **2018**, *808*, 286−292.
(28) Abbasi, F.; Leitch, J. J.; Su, Z.; Szymanski, G.; Lipkowski, J. Direct Visualization of Alamethicin Ion Pores Formed in a Floating Phospholipid Membrane Supported on a Gold Electrode surface. *Electrochim. Acta* **2018**, *267*, 195−205.
(29) Juhaniewicz, J.; Sek, S. Atomic Force Microscopy and Electrochemical Studies of Melittin Action on Lipid Bilayers Supported on Gold Electrodes. *Electrochim. Acta* **2015**, *162*, 53−61.
(30) Cannes, C.; Kanoufi, F.; Bard, A. J. Cyclic Voltammetry and Scanning Electrochemical Microscopy of Ferrocenemethanol at Monolayer and Bilayer-modified Gold Electrodes. *J. Electroanal. Chem.* **2003**, *547*, 83−91.
(31) Zawisza, I.; Bin, X.; Lipkowski, J. Spectroelectrochemical Studies of Bilayers of Phospholipids in Gel and Liquid State on Au(111) Electrode Surface. *Bioelectrochemistry* **2004**, *63*, 137−147.
(32) Burgess, I.; Li, M.; Horswell, S. L.; Szymanski, G.; Lipkowski, J.; Majewski, J.; Satija, S. Electric Field-Driven Transformations of a Supported Model Biological Membrane-An Electrochemical and Neutron Reflectivity Study. *Biophys. J.* **2004**, *86*, 1763−1776.
(33) Lipkowski, J. Building Biomimetic Membrane at a Gold Electrode Surface. *Phys. Chem. Chem. Phys.* **2010**, *12*, 13874−13887.
(34) Burgess, I.; Li, M.; Horswell, S. L.; Szymanski, G.; Lipkowski, J.; Satija, S.; Majewski, J. Influence of the Electric Field on a Bio-mimetic Film Supported on a Gold Electrode. *Colloids Surf., B* **2005**, *40*, 117−122.
(35) Krysinski, P.; Moncelli, M. R.; Tadini-Buoninsegni, F. A Voltammetric Study of Monolayers and Bilayers Self-assembled on Metal Electrodes. *Electrochim. Acta* **2000**, *45*, 1885−1892.
(36) Li, M.; Chen, M.; Sheepwash, E.; Brosseau, C. L.; Li, H.; Pettinger, B.; Gruler, H.; Lipkowski, J. AFM Studies of Solid-Supported Lipid Bilayers Formed at a Au(111) Electrode Surface Using Vesicle Fusion and a Combination of Langmuir−Blodgett and Langmuir−Schaefer Techniques. *Langmuir* **2008**, *24*, 10313−10323.
(37) Kycia, A. H.; Wang, J.; Merrill, A. R.; Lipkowski, J. Atomic Force Microscopy Studies of a Floating-Bilayer Lipid Membrane on a Au(111) Surface Modified with a Hydrophilic Monolayer. *Langmuir* **2011**, *27*, 10867−10877.
(38) Donaldson, S. H.; Valtiner, M.; Gebbie, M. A.; Harada, J.; Israelachvili, J. N. Interactions and Visualization of Bio-mimetic Membrane Detachment at Smooth and Nano-rough Gold Electrode Surfaces. *Soft Matter* **2013**, *9*, 5231−5238.
(39) Matyszewska, D.; Sek, S.; Jabłonowska, E.; Pałys, B.; Pawlowski, J.; Bilewicz, R.; Konrad, F.; Osornio, Y. M.; Landau, E. M. Dependence of Interfacial Film Organization on Lipid Molecular Structure. *Langmuir* **2014**, *30*, 11329−11339.
(40) Gutiérrez-Sánchez, C.; Olea, D.; Marques, M.; Fernández, V. M.; Pereira, I. A. C.; Vélez, M.; De Lacey, A. L. Oriented Immobilization of a Membrane-Bound Hydrogenase onto an Electrode for Direct Electron Transfer. *Langmuir* **2011**, *27*, 6449−6457.
(41) Marquês, J. T.; de Almeida, R. F. M.; Viana, A. S. Biomimetic Membrane Rafts Stably Supported on Unmodified Gold. *Soft Matter* **2012**, *8*, 2007−2016.
(42) Ip, S.; Li, J. K.; Walker, G. C. Phase Segregation of Untethered Zwitterionic Model Lipid Bilayers Observed on Mercaptoundecanoic-Acid-Modified Gold by AFM Imaging and Force Mapping. *Langmuir* **2010**, *26*, 11060−11070.
(43) Kocábová, J.; Kolivoška, V.; Gál, M.; Sokolová, R. Tuning phospholipid bilayer permeability by flavonoid apigenin: Electrochemical and atomic force microscopy study. *J. Electroanal. Chem.* **2018**, *821*, 67−72.
(44) Brukhno, A. V.; Akinshina, A.; Coldrick, Z.; Nelson, A.; Auer, S. Phase Phenomena in Supported Lipid Films under Varying Electric Potential. *Soft Matter* **2011**, *7*, 1006−1017.
(45) Leermakers, F. A. M.; Nelson, A. Substrate-induced structural changes in electrode-adsorbed lipid layers. *J. Electroanal. Chem.* **1990**, *278*, 53−72.
(46) Nelson, A.; Leermakers, F. A. M. Substrate-induced structural changes in electrode-adsorbed lipid layers. *J. Electroanal. Chem.* **1990**, *278*, 73−83.
(47) Monné, J.; Díez, Y.; Puy, J.; Galceran, J.; Nelson, A. Interpreting Ion Fluxes to Channel Arrays in Monolayers. *Langmuir* **2007**, *23*, 10581−10588.
(48) Nelson, A. Conducting Gramicidin Channel Activity in Phospholipid Monolayers. *Biophys. J.* **2001**, *80*, 2694−2703.
(49) Nelson, A. Electrochemistry of Mercury Supported Phospholipid Monolayers and Bilayers. *Curr. Opin. Colloid Interface Sci.* **2010**, *15*, 455−466.
(50) Whitehouse, C.; O'Flanagan, R.; Lindholm-Sethson, B.; Movaghar, B.; Nelson, A. Application of Electrochemical Impedance Spectroscopy to the Study of Dioleoyl Phosphatidylcholine Monolayers on Mercury. *Langmuir* **2004**, *20*, 136−144.
(51) Bizzotto, D.; Yang, Y.; Shepherd, J. L.; Stoodley, R.; Agak, J.; Stauffer, V.; Lathuillière, M.; Akhtar, A. S.; Chung, E. Electrochemical and Spectroelectrochemical Characterization of Lipid Organization in an Electric Field. *J. Electroanal. Chem.* **2004**, *574*, 167−184.
(52) Gao, X.; White, H. S.; Chen, S.; Abruna, H. D. Electric-Field-Induced Transitions of Amphiphilic Layers on Mercury Electrodes. *Langmuir* **1995**, *11*, 4554−4563.
(53) Herrero, R.; Barriada, J. L.; López-Fonseca, J. M.; Moncelli, M. R.; Sastre de Vicente, M. E. Effect of Ionic Strength on the Electrochemical Behavior of Glutathione on a Phospholipid Self-Assembled Monolayer on Mercury. *Langmuir* **2000**, *16*, 5148−5153.
(54) Mauzeroll, J.; Buda, M.; Bard, A. J.; Prieto, F.; Rueda, M. Detection of Tl(I) Transport through a Gramicidin−Dioleoylphosphatidylcholine Monolayer Using the Substrate Generation−Tip Collection Mode of Scanning Electrochemical Microscopy. *Langmuir* **2002**, *18*, 9453−9461.
(55) Coldrick, Z.; Steenson, P.; Millner, P.; Davies, M.; Nelson, A. Phospholipid Monolayer Coated Microfabricated Electrodes to Model the Interaction of Molecules with Biomembranes. *Electrochim. Acta* **2009**, *54*, 4954−4962.
(56) Coldrick, Z.; Penezić, A.; Gašparović, B.; Steenson, P.; Merrifield, J.; Nelson, A. High Throughput Systems for Screening Biomembrane Interactions on Fabricated Mercury Film Electrodes. *J. Appl. Electrochem.* **2011**, *41*, 939−949.
(57) Nelson, A. Electrochemical analysis of a phospholipid phase transition. *J. Electroanal. Chem.* **2007**, *601*, 83−93.
(58) Vakurov, A.; Galluzzi, M.; Podestà, A.; Gamper, N.; Nelson, A. L.; Connell, S. D. A. Direct Characterization of Fluid Lipid Assemblies on Mercury in Electric Fields. *ACS Nano* **2014**, *8*, 3242−3250.
(59) Stoodley, R.; Bizzotto, D. Epi-fluorescence Microscopic Characterization of Potential-Induced Changes in a DOPC Monolayer on a Hg Drop. *Analyst* **2003**, *128*, 552−561.
(60) Mustata, G.-M.; Kim, Y. H.; Zhang, J.; DeGrado, W. F.; Grigoryan, G.; Wanunu, M. Graphene Symmetry Amplified by Designed Peptide Self-Assembly. *Biophys. J.* **2016**, *110*, 2507−2516.
(61) Hayamizu, Y.; So, C. R.; Dag, S.; Page, T. S.; Starkebaum, D.; Sarikaya, M. Bioelectronic Interfaces by Spontaneously Organized Peptides on 2D Atomic Single Layer Materials. *Sci. Rep.* **2016**, *6*, 33778.
(62) Seki, T.; So, C. R.; Page, T. R.; Starkebaum, D.; Hayamizu, Y.; Sarikaya, M. Electrochemical Control of Peptide Self-Organization on Atomically Flat Solid Surfaces: A Case Study with Graphite. *Langmuir* **2017**, *34*, 1819−1826.
(63) Piantanida, L.; Bolt, H. L.; Rozatian, N.; Cobb, S. L.; Voïtchovsky, K. Ions Modulate Stress-Induced Nanotexture in Supported Fluid Lipid Bilayers. *Biophys. J.* **2017**, *113*, 426−439.
(64) Voïtchovsky, K.; Giofrè, D.; José Segura, J.; Stellacci, F.; Ceriotti, M. Thermally-nucleated Self-assembly of Water and Alcohol into Stable Structures at Hydrophobic Interfaces. *Nat. Commun.* **2016**, *7*, 13064.

DOI: 10.1021/acs.langmuir.8b01631
Langmuir XXXX, XXX, XXX−XXX

(65) Ricci, M.; Quinlan, R. A.; Voïtchovsky, K. Sub-nanometre Mapping of the Aquaporin-Water Interface using Multifrequency Atomic Force Microscopy. *Soft Matter* **2017**, *13*, 187−195.
(66) Ricci, M.; Trewby, W.; Cafolla, C.; Voitchovsky, K. Direct Observation of the Dynamics of Single Metal ions at the Interface with Solids in Aqueous Solutions. *Sci. Rep.* **2017**, *7*, 43234.
(67) Trewby, W.; Livesey, D.; Voïtchovsky, K. Buffering Agents Modify the Hydration Landscape at Charged Interfaces. *Soft Matter* **2016**, *12*, 2642−2651.
(68) Mingeot-Leclercq, M.-P.; Deleu, M.; Brasseur, R.; Dufrêne, Y. F. Atomic Force Microscopy of Supported Lipid Bilayers. *Nat. Protoc.* **2008**, *3*, 1654−1659.
(69) Richter, R. P.; Bérat, R.; Brisson, A. R. Formation of Solid-supported Lipid Bilayers: an Integrated View. *Langmuir* **2006**, *22*, 3497−3505.
(70) Wang, X.; Zhang, Y.; Bi, H.; Han, X. Supported Lipid Bilayer Membrane Arrays on Micro-patterned ITO Electrodes. *RSC Adv.* **2016**, *6*, 72821−72826.
(71) Miller, E. J.; Trewby, W.; Payam, A. F.; Piantanida, L.; Cafolla, C.; Voïtchovsky, K. Sub-nanometer Resolution Imaging with Amplitude-modulation Atomic Force Microscopy in Liquid. *J. Visualized Exp.* **2016**, *118*, e54924.
(72) Voïtchovsky, K. Anharmonicity, solvation forces, and resolution in atomic force microscopy at the solid-liquid interface. *Phys. Rev. E: Stat., Nonlinear, Soft Matter Phys.* **2013**, *88*, 022407.
(73) Schneider, C. A.; Rasband, W. S.; Eliceiri, K. W. NIH Image to ImageJ: 25 years of image analysis. *Methods* **2012**, *9*, 671−675.
(74) Soumpasis, D. M. Theoretical Analysis of Fluorescence Photobleaching Recovery Experiments. *Biophys. J.* **1983**, *41*, 95−97.
(75) McKiernan, A. E.; Ratto, T. V.; Longo, M. L. Domain Growth, Shapes, and Topology in Cationic Lipid Bilayers on Mica by Fluorescence and Atomic Force Microscopy. *Biophys. J.* **2000**, *79*, 2605−2615.
(76) Kang, M.; Day, C. A.; Kenworthy, A. K.; DiBenedetto, E. Simplified Equation to Extract Diffusion Coefficients from Confocal FRAP Data. *Traffic* **2012**, *13*, 1589−1600.
(77) Blumenthal, D.; Goldstien, L.; Edidin, M.; Gheber, L. A. Universal Approach to FRAP Analysis of Arbitrary Bleaching Patterns. *Sci. Rep.* **2015**, *5*, 11655.
(78) Zawisza, I.; Bin, X.; Lipkowski, J. Potential-Driven Structural Changes in Langmuir−Blodgett DMPC Bilayers Determined by in situ Spectroelectrochemical PM IRRAS. *Langmuir* **2007**, *23*, 5180−5194.
(79) Wang, B.; Zhang, L.; Bae, S. C.; Granick, S. Nanoparticle-induced Surface Reconstruction of Phospholipid Membranes. *Proc. Natl. Acad. Sci. U.S.A.* **2008**, *105*, 18171−18175.
(80) Guriyanova, S.; Mairanovsky, V. G.; Bonaccurso, E. Super-viscosity and Electroviscous Effects at an Electrode/aqueous Electrolyte Interface: An Atomic Force Microscope Study. *J. Colloid Interface Sci.* **2011**, *360*, 800−804.
(81) Wang, J. J.; Li, T.; Bateman, S. D.; Erck, R.; Morris, K. R. Modeling of Adhesion in Tablet Compression-I. Atomic Force Microscopy and Molecular Simulation. *J. Pharm. Sci.* **2003**, *92*, 798−814.
(82) Obst, M.; Dittrich, M.; Kuehn, H. Calcium Adsorption and Changes of the Surface Microtopography of Cyanobacteria Studied by AFM, CFM, and TEM with Respect to Biogenic Calcite Nucleation. *Geochem., Geophys., Geosyst.* **2006**, *7*, Q06011.
(83) Peng, H.; Birkett, G. R.; Nguyen, A. V. Origin of Interfacial Nanoscopic Gaseous Domains and Formation of Dense Gas Layer at Hydrophobic Solid-Water Interface. *Langmuir* **2013**, *29*, 15266−15274.
(84) Lenz, P.; Ajo-Franklin, C. M.; Boxer, S. G. Patterned Supported Lipid Bilayers and Monolayers on Poly(dimethylsiloxane). *Langmuir* **2004**, *20*, 11092−11099.
(85) Montal, M.; Mueller, P. Formation of bimolecular membranes from lipid monolayers and a study of their electrical properties. *Proc. Natl. Acad. Sci. U.S.A.* **1972**, *69*, 3561−3566.
(86) Römer, W.; Steinem, C. Impedance analysis and single-channel recordings on nano-black lipid membranes based on porous alumina. *Biophys. J.* **2004**, *86*, 955−965.
(87) Xu, S.; Szymanski, G.; Lipkowski, J. Self-assembly of phospholipid molecules at a Au(111) electrode surface. *J. Am. Chem. Soc.* **2004**, *126*, 12276−12277.
(88) Petri, M.; Kolb, D. M. Nanostructuring of a sodium dodecyl sulfate-covered Au(111) electrode. *Phys. Chem. Chem. Phys.* **2002**, *4*, 1211−1216.
(89) Pawłowski, J.; Juhaniewicz, J.; Güzeloğlu, A.; Sęk, S. Mechanism of Lipid Vesicles Spreading and Bilayer Formation on a Au(111) Surface. *Langmuir* **2015**, *31*, 11012−11019.
(90) Matsunaga, S.; Shimizu, H.; Yamada, T.; Kobayashi, T.; Kawai, M. In Situ STM and Vibrational Study of Nanometer-Scale Reorganization of a Phospholipid Monolayer Accompanied by Potential-Driven Headgroup Digestion. *Langmuir* **2017**, *33*, 13157−13167.
(91) Casal, H. L.; Mantsch, H. H.; Hauser, H. Infrared studies of fully hydrated saturated phosphatidylserine bilayers. Effect of lithium and calcium. *Biochemistry* **1987**, *26*, 4408−4416.
(92) Zhang, Y.; Wang, X.; Ma, S.; Jiang, K.; Han, X. Lipid Membrane Formation on Chemical Gradient Modified Surfaces. *RSC Adv.* **2016**, *6*, 11325−11328.
(93) Sedlmeier, F.; von Hansen, Y.; Mengyu, L.; Horinek, D.; Netz, R. R. Water Dynamics at Interfaces and Solutes: Disentangling Free Energy and Diffusivity Contributions. *J. Stat. Phys.* **2011**, *145*, 240−252.
(94) Toppozini, L.; Roosen-Runge, F.; I. Bewley, R.; M. Dalgliesh, R.; Perring, T.; Seydel, T.; Glyde, H. R.; García Sakai, V.; Rheinstädter, M. C. Anomalous and Anisotropic Nanoscale Diffusion of Hydration Water Molecules in Fluid Lipid Membranes. *Soft Matter* **2015**, *11*, 8354−8371.
(95) Von Hansen, Y.; Gekle, S.; Netz, R. R. Anomalous Anisotropic Diffusion Dynamics of Hydration Water at Lipid Membranes. *Phys. Rev. Lett.* **2013**, *111*, 118103.
(96) Charrier, A.; Thibaudau, F. Main Phase Transitions in Supported Lipid Single-bilayer. *Biophys. J.* **2005**, *89*, 1094−1101.
(97) Alessandrini, A.; Seeger, H. M.; Di Cerbo, A.; Caramaschi, T.; Facci, P. What do We Really Measure in AFM Punch-through Experiments on Supported Lipid Bilayers? *Soft Matter* **2011**, *7*, 7054−7064.
(98) Yesylevskyy, S. O.; Ramseyer, C. Determination of Mean and Gaussian Curvatures of Highly Curved Asymmetric Lipid Bilayers: the Case Study of the Influence of Cholesterol on the Membrane Shape. *Phys. Chem. Chem. Phys.* **2014**, *16*, 17052−17061.
(99) Frotscher, E.; Danielczak, B.; Vargas, C.; Meister, A.; Durand, G.; Keller, S. A Fluorinated Detergent for Membrane-Protein Applications. *Angew. Chem., Int. Ed.* **2015**, *54*, 5069−5073.
(100) Grison, M. S.; Brocard, L.; Fouillen, L.; Nicolas, W.; Wewer, V.; Dörmann, P.; Nacir, H.; Benitez-Alfonso, Y.; Claverol, S.; Germain, V.; Boutté, Y.; Mongrand, S.; Bayer, E. M. Specific Membrane Lipid Composition Is Important for Plasmodesmata Function in Arabidopsis. *Plant Cell* **2015**, *27*, 1228−1250.
(101) Matsunaga, S.; Yokomori, R.; Ino, D.; Yamada, T.; Kawai, M.; Kobayshi, T. EC-STM observation on electrochemical response of fluidic phospholipid monolayer on Au(111) modified with 1-octanethiol. *Electrochem. Commun.* **2007**, *9*, 645−650.

DOI: 10.1021/acs.langmuir.8b01631
Langmuir XXXX, XXX, XXX−XXX